



Contents lists available at ScienceDirect

## Journal of Volcanology and Geothermal Research

journal homepage: [www.elsevier.com/locate/jvolgeores](http://www.elsevier.com/locate/jvolgeores)

## Dynamics of mild strombolian activity on Mt. Etna

T.D. Pering<sup>a,\*</sup>, G. Tamburello<sup>b</sup>, A.J.S. McGonigle<sup>a,c</sup>, A. Aiuppa<sup>b,c</sup>, M.R. James<sup>d</sup>, S.J. Lane<sup>d</sup>, M. Sciotto<sup>e</sup>, A. Cannata<sup>e</sup>, D. Patanè<sup>e</sup><sup>a</sup> University of Sheffield, Dept. of Geography, Winter Street, S10 2TN, UK<sup>b</sup> DiSTeM, Università di Palermo, via Archirafi, 22, 90123 Palermo, Italy<sup>c</sup> Istituto Nazionale di Geofisica e Vulcanologia, Sezione di Palermo, Via Ugo La Malfa, 153, 90146 Palermo, Italy<sup>d</sup> Lancaster Environment Centre, Lancaster University, Lancaster LA1 4YQ, UK<sup>e</sup> Istituto Nazionale di Geofisica e Vulcanologia, Osservatorio Etneo, Piazza Roma, 2, 95125,11 Catania, Italy

## ARTICLE INFO

## Article history:

Received 3 April 2014

Accepted 16 December 2014

Available online xxxxx

## Keywords:

Mild strombolian activity

Ultra-violet imaging

Volcanic gas measurements

Slug dynamics

Coalescence

Trailing wake interaction

## ABSTRACT

Here we report the first measurements of gas masses released during a rare period of strombolian activity at the Bocca Nuova crater, Mt. Etna, Sicily. UV camera data acquired for 195 events over an  $\approx 27$  minute period (27th July 2012) indicate erupted  $\text{SO}_2$  masses ranging from  $\approx 0.1$  to  $\approx 14$  kg per event, with corresponding total gas masses of  $\approx 0.1$  to 74 kg. Thus, the activity was characterised by more frequent and smaller events than typically associated with strombolian activity on volcanoes such as Stromboli. Events releasing larger measured gas masses were followed by relatively long repose periods before the following burst, a feature not previously reported on from gas measurement data. If we assume that gas transport within the magma can be represented by a train of rising gas pockets or slugs, then the high frequency of events indicates that these slugs must have been in close proximity. In this case the longer repose durations associated with the larger slugs would be consistent with interactions between adjacent slugs leading to coalescence, a process expedited close to the surface by rapid slug expansion. We apply basic modelling considerations to the measured gas masses in order to investigate potential slug characteristics governing the observed activity. We also cross correlated the acquired gas fluxes with contemporaneously obtained seismic data but found no relationship between the series in line with the mild form of manifest explosivity.

© 2014 Elsevier B.V. All rights reserved.

## 1. Introduction

Strombolian eruptions are thought to arise from the rise, expansion and bursting of over-pressured gas slugs, also termed Taylor bubbles (e.g., Chouet et al., 1974; Blackburn et al., 1976; Wilson, 1980; Vergnolle and Brandeis, 1994, 1996; Ripepe et al., 2008). The behaviour of single slugs, where the rising bubbles are sufficiently separated from one another to behave independently, has received considerable attention in the volcanological and fluid dynamical literature (e.g. Davies and Taylor, 1950; Wallis, 1969; James et al., 2008, 2009; Llewellyn et al., 2012). Indeed, theoretical frameworks have been developed to link observed geophysical signals to the characteristics of single volcanic slugs (James et al., 2009; Llewellyn et al., 2012; Lane et al., 2013). In contrast, only a few studies have addressed the behaviour of multiple slugs in volcanic regimes (Seyfried and Freundt, 2000; James et al., 2004; Pioli et al., 2012) given the additional complexities involved.

Recently developed UV camera technology (e.g., Mori and Burton, 2006; Bluth et al., 2007; Tamburello et al., 2011a) has provided considerably enhanced spatial and temporal resolutions ( $\approx 1$  Hz) in the acquisition of volcanic  $\text{SO}_2$  degassing time-series, relative to previously applied spectroscopic approaches (Edmonds et al., 2003; Galle et al., 2003; Burton et al., 2009; Boichu et al., 2010). The acquired data have therefore led to increased understanding of a number of explosive and passive degassing volcanic phenomena, for example, the degassing mechanism in the Santiaguito lava dome, Guatemala (Holland et al., 2011), the links between gas flux trends and seismicity during passive degassing (Tamburello et al., 2013; Pering et al., 2014), the relationship between gas emissions and very-long-period seismicity at Mt. Asama, Japan (Kazahaya et al., 2011), and the ties between gas emissions and generated infrasonic energy (Dalton et al., 2010).

UV camera imagery, in addition to FTIR (Fourier Transform Infrared) spectroscopy has also been used to investigate the dynamics of gas release from single slug driven strombolian activity on targets such as Stromboli (Aeolian Islands, Italy) (e.g., Burton et al., 2007; Mori and Burton, 2009; Tamburello et al., 2012; La Spina et al., 2013). This has led to constraints on the gas mass released per event, and the slugs' source depth. In contrast to Stromboli, where this activity is

\* Corresponding author at: Department of Geography, University of Sheffield, Sheffield, South Yorkshire S10 2TN, UK.

E-mail address: [ggp12tdp@sheffield.ac.uk](mailto:ggp12tdp@sheffield.ac.uk) (T.D. Pering).

quasi-continuous, such behaviour occurs only sporadically on Mt. Etna (Sicily, Italy).

Here we report on the first application of UV camera imaging to measure gas masses from strombolian activity on Mt. Etna, during a very rare period of this style of activity at the Bocca Nuova (BN) crater. Indeed, prior to our observations, on the 27th of July 2012 there had only been two previous episodes of strombolian activity from BN in the preceding decade, in 2002 and 2011, respectively (GVP, 2013). The acquired degassing data were analysed within the physical framework developed by previous studies concerning slug flow, in order to seek new insights into the conduit fluid dynamics.

## 2. Bocca Nuova activity, 27th July 2012

During the measurement period, activity on Etna was dominated by strombolian explosions from a vent in the south-west corner of the BN crater (Fig. 1,  $\approx$  N 37.7503°, E 14.9936° see Supplementary materials for a .kmz file containing all relevant measurement locations). Each event lasted <4 s, was ash-free, involving a single audible bang, ballistic ejection of only a small number of visible pyroclasts (e.g. see Supplementary video), and the subsequent rapid emission of gases. The largest clasts were observed to deform in a ductile fashion in flight. Between explosions, the vent passively degassed (e.g., see Fig. 2a and video in the Supplementary material). This vent generated explosions throughout the majority of July 2012, in addition to small lava flows (GVP, 2013). During the measurement period, prevailing winds at the crater edge carried the gas emissions in an E-SE direction (see Fig. 1).

## 3. Methodology

SO<sub>2</sub> fluxes from the BN vent were measured between 09:32:58 and 09:59:58 GMT on July 27th, 2012, with two PC-synchronised Apogee-AltA U260 UV cameras, each fitted with a 16 bit 512 × 512 pixel Kodak

KAF-0261E thermo-electrically cooled CCD array detector. Each camera had a Pentax B2528-UV lens with a focal length of 25 mm, providing an  $\approx$ 24° field of view. A filter was placed in front of each lens, one centred on 310 nm and the other on 330 nm, and each of 10 nm full width at half maximum transmission bandwidth. As SO<sub>2</sub> absorbs in the 310 nm wavelength region, but not at 330 nm, a pair of simultaneously acquired images from the cameras can be processed to yield absorbance values. The data capture and analysis were achieved using the Vulcamera code (Tamburello et al., 2011b) and full details on the methodology are covered in Kantzas et al. (2010).

The UV camera apparatus was located as denoted in Fig. 1,  $\approx$ 250 m from the vent (N 37.7525°, E 14.9950°), providing the view of the BN crater shown in Fig. 2a and care was exercised to position the cameras away from potential contamination by gases from other sources; the acquisition frequency was  $\approx$  1 Hz. Given this close proximity to the source we anticipate that error arising from light dilution was small; e.g., from scattering of radiation from outside of the instrumental field of view to within it, i.e., between the camera and the measured vent area, an error source which could potentially lead to an underestimation in measured column amount values. This being said, it is not possible at this stage to assign a definitive characterisation of measurement error from this effect, as radiative transfer has yet to become a routine component of UV camera retrievals (e.g., Kern et al., 2009, 2010). The same is true of light scattering within the plume, which could potentially act to cause overestimation in concentration values.

### 3.1. Camera calibration

To calibrate the system, cells of known concentrations (100, 200, 400, 1600 ppm m with manufacturer stated error budgets of  $\pm$  50 ppm m, and  $\pm$  100 ppm m for the 400 ppm m and 1600 ppm m cells, respectively) were placed in front of the cameras in sequence, and the absorbances determined. In our measurements, the image background was the

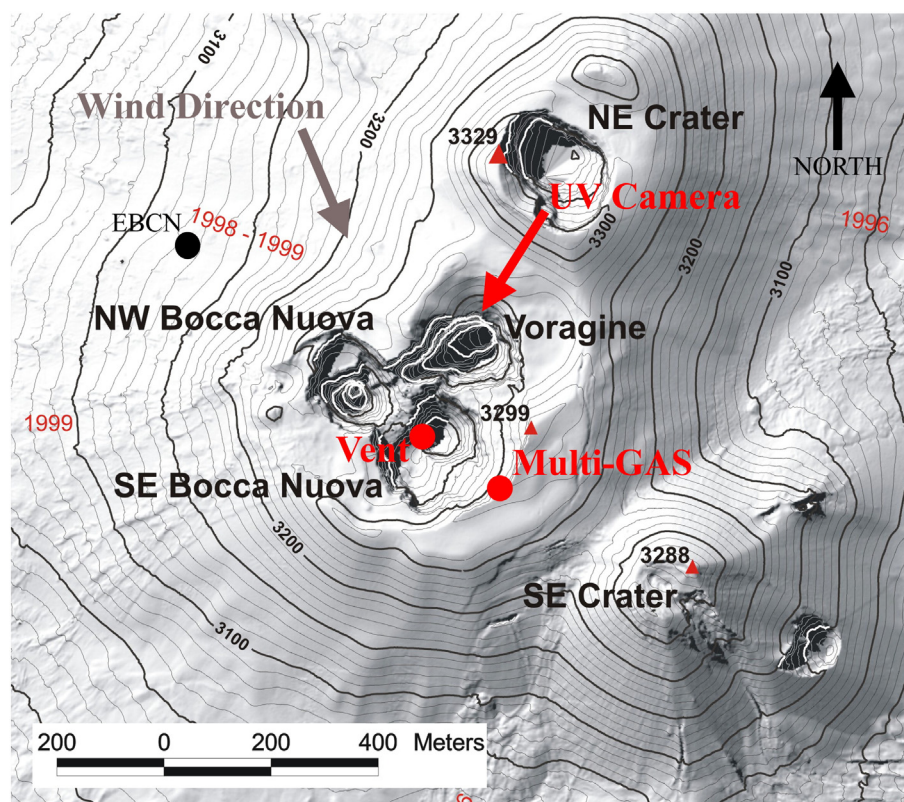
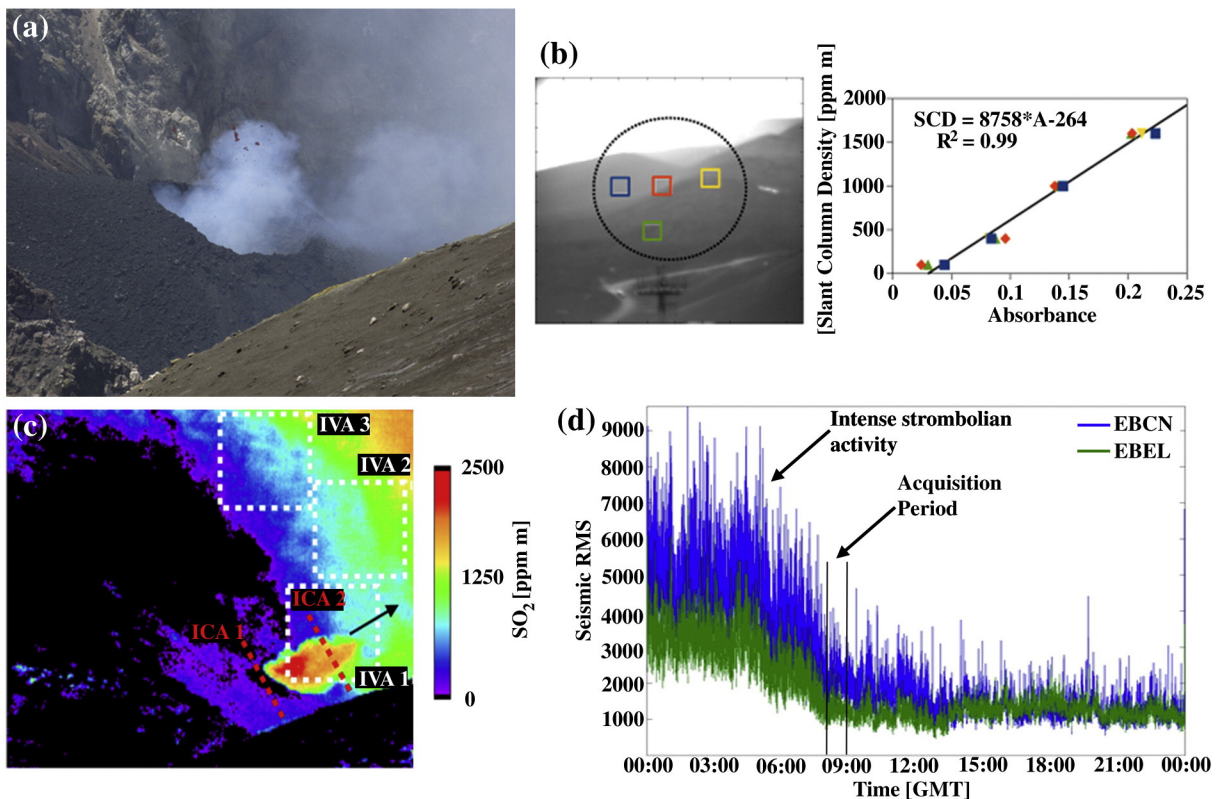


Fig. 1. Map of Mt. Etna's summit showing the BN vent (red circle), the UV camera location (end of the red arrow), the Multi-GAS location, the wind direction (grey arrow) and the seismic station EBCN (black circle). (For interpretation of the references to colour in this figure legend, the reader is referred to the web version of this article.)



**Fig. 2.** a) Strombolian activity from the vent at the south-west corner of Bocca Nuova; image taken at the time and location of our acquisitions; b) gas free 310 nm camera image showing four pixel regions used to investigate the angular variation in cell calibrations using rock as the measurement background; the resulting plotted calibration data (cell concentration vs. measured absorbance with points colour matched to the corresponding pixel region) show good agreement between the four regions and a collective  $R^2 > 0.99$ ; c) UV camera gas concentration image of BN showing IVA1, the area used to determine erupted gas masses with reference to two background areas: IVA2 and IVA3, and ICA1 and ICA2, which were used to calculate gas emission rates as detailed in the main text; and d) seismic RMS from stations EBCN and EBEL throughout July 27th 2012 (ETFI omitted to provide greater figure clarity), showing the period of intense Strombolian activity.

basaltic rock face of the BN crater wall, as opposed to the sky, which is more conventionally used for such observations. Hence, the calibration, vignetting correction (an essential step in removing the inhomogeneous illumination of the detector across the field-of-view) and reference image acquisition steps (see Kantzas et al., 2010 for full details) of the measurement were performed by viewing the crater wall through air with minimal  $\text{SO}_2$  concentration, adjacent to the rising gas plume. A rock-reflectance light source approach is also commonly used in the study of planetary surface bodies (e.g. Hendrix et al., 2003) and in our case, this provided around 40% of the UV light intensity of the background sky immediately above the crater, e.g., a sufficiently strong source for our observations. The measurement location was also free from fumarolic contamination and unaffected by gases sourced from other craters.

Given the variation in light scattering orientation from the background basaltic rock across the camera field of view, we also investigated whether any angular dependency in cell calibration across the image might be introduced due to this effect. This was achieved by imaging an  $\text{SO}_2$  free region with a basaltic rock background in the Etnan summit area with illumination conditions as similar as possible to those during the measurements (e.g., there was a thin strip of sky in the uppermost region of the images). In particular we tested whether calibration could be skewed over the angular difference between the plume gases and the adjacent background rock viewing orientations in our measurements ( $\approx 12^\circ$ ) by determining calibration lines for a number of data points in the  $\text{SO}_2$  free image within this diameter of the image centre (Fig. 2b). Plotted together (Fig. 2b) the calibration data points reveal very similar calibration gradients in all cases, with an overall  $R^2 = 0.99$ , leading us to exclude the possibility of this effect introducing significant error.

### 3.2. Data processing

The data analysis firstly involved detecting Strombolian explosion events in the UV camera records by identifying when the gas emission speed markedly increased and solid ejecta were identifiable. For each such event  $\text{SO}_2$  gas masses were derived from the processed UV camera  $\text{SO}_2$  concentration images using the integrated volume amount (IVA) technique (Tamburello et al., 2012). With this approach, gas concentrations were integrated within an appropriately chosen 2D subsection of the image immediately above the vent, of sufficient size to encompass the explosive clouds to generate the IVA (Fig. 2c). Fig. 3 shows the gas cloud propagation over five consecutive images following one such explosion, showing wireframe sketches (Fig. 3a–e) of the advancing cloud, the cloud vector of motion and the IVA integration area.

These IVAs require correction for background  $\text{SO}_2$  levels associated with the collection of gases within BN following emission, as the spatial location of these varied temporally throughout the acquisition in response to changing atmospheric conditions. Background correction was achieved by determining integrated  $\text{SO}_2$  concentrations for two subsections of the image, adjacent to the explosion, and of identical dimensions to the area used in the explosion cloud 2D integration (Fig. 2c). The explosion IVA was then corrected by subtracting the average of the masses within these two background areas which typically agreed with one another to within  $\approx 6\%$ . For each event, the temporal peak in the corrected IVA record was identified, then integration was performed between the event onset and event termination to yield the explosive gas mass. For reference, video material is provided in the auxiliary materials showing two acquired UV camera image time series.

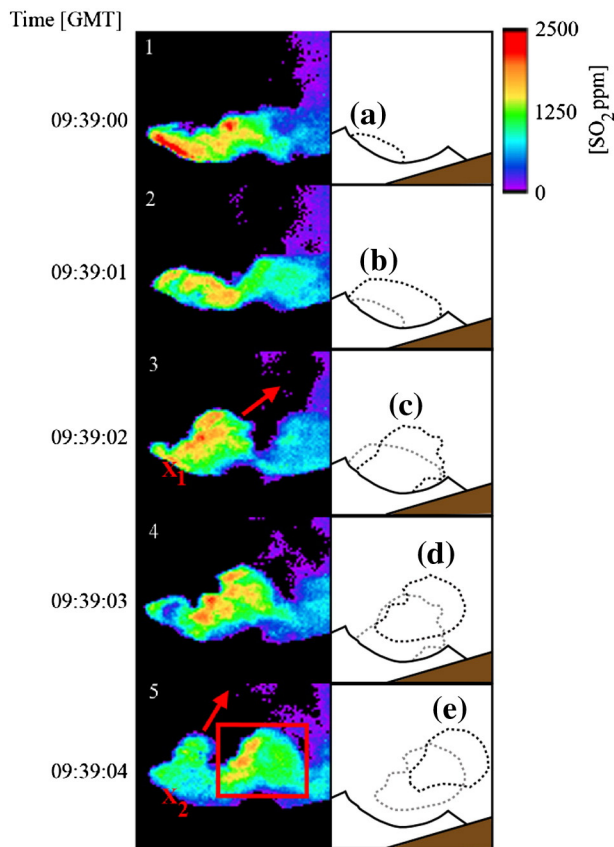


**Fig. 3.** A sequence of cropped UV camera gas concentration images to illustrate a single strombolian event and determination of  $\text{SO}_2$  concentration (images 1–5); alongside are wireframe representations of the burst front for each image (a–e); the red box indicates the area used to produce the integrated volume amount (IVA) from Fig. 2c; and red arrows indicate two distinct burst vectors for the main burst in images 1–5 and a subsequent burst in image 5, respectively which with points x1 and x2 denoting two burst origins. (For interpretation of the references to colour in this figure legend, the reader is referred to the web version of this article.)

These data were then applied to investigate total slug masses, using contemporaneously acquired Multi-GAS (Aiuppa et al., 2007) gas ratio data from a unit deployed by INGV (Istituto Nazionale di Geofisica e Vulcanologia) sezione di Palermo. The Multi-GAS unit was located on the crater's edge at the site shown in Fig. 1 (N 37.7409°, E 14.9953°) at a distance of  $\approx 200$  m from the active vent and away from possible contamination sources; the wind direction and speed were E-SE and  $10\text{--}14\text{ m s}^{-1}$ , respectively. Averaged over the acquisition period, the measured Multi-GAS molar ratios were:  $\text{CO}_2/\text{SO}_2 \approx 2.8$ ;  $\text{H}_2\text{O}/\text{SO}_2 \approx 8.5$ ; and  $\text{H}_2\text{O}/\text{CO}_2 \approx 3$ . Temporal averaging was applied due to the difficulty of isolating individual explosive events in the Multi-GAS record resulting from the spatial separation of the vent and the Multi-GAS unit and the time resolution of the Multi-GAS data (0.5 Hz). During the entire acquisition, the ratios were relatively stable (with errors on gas ratios of  $\approx 4\text{--}15\%$  e.g. Pering et al., 2014), and total gas masses were calculated based on the assumption that  $\text{H}_2\text{O}$ ,  $\text{CO}_2$ , and  $\text{SO}_2$  dominated the plume composition (e.g., Aiuppa et al., 2007). The molar plume composition was therefore taken to be 8%  $\text{SO}_2$ , 22%  $\text{CO}_2$  and 70%  $\text{H}_2\text{O}$  from the Multi-GAS measurements, on which basis the explosive  $\text{SO}_2$  gas masses were converted, via multiplication, using the respective mass ratios, to total gas release per event. However, it is likely, as per previous studies at similar targets (e.g. Burton et al., 2007; Tamburello et al., 2012), that the gas compositions from the passive and explosive contributions were non-identical. Our determined total gas masses are therefore best-estimates given the data available.

A gas flux time series was also constrained by summing the image concentrations over a cross section above the vent (Fig. 2c) to generate an integrated column amount (ICA) data-stream, then multiplying this by the plume speed, projected onto a vector perpendicular to this cross section. The inter-event plume rise speed was determined using a cross correlation technique on ICA data derived from two parallel sections of the rising plume, in periods after the increase in emission speed associated with gas explosions had subsided (e.g., McGonigle et al., 2005; Williams-Jones et al., 2006), with results of  $\approx 5\text{ m s}^{-1}$ . During the explosions themselves the plume speed was constrained by frame tracking of the cloud front across the camera field of view.

### 3.3. Seismicity

The potential relationship between gas flux and seismic RMS (root-mean-square) was investigated using signals recorded by three seismic stations (EBCN N 37.752365° E 14.986281°; ETFI N 37.738195°, E 15.000649°; and EBEL N 37.740238° E 15.008239°; see Fig. 1 for EBCN location) belonging to the permanent network, run by INGV, Osservatorio Etneo - sezione di Catania. Since these stations are located close to the summit craters ( $\approx 1$  km away from the centre of the summit area), the seismic RMS patterns were mostly affected by the temporal variations of volcanic tremor, long period (LP) and very long period (VLP) events. The seismic RMS was calculated over windows of 2, 5, 10 and 30 s in two distinct frequency bands: 0.05–0.5 Hz and 0.5–5.0 Hz. These bands were chosen because they contain most of the energy of the seismo-volcanic signals (volcanic tremor, LP and VLP events) at Mt. Etna (e.g., Cannata et al., 2013). Fig. 2d shows the seismic RMS time series preceding, accompanying and following the UV camera acquisition period. The comparison between seismic RMS and the gas flux data was performed using the method of Martini et al. (2009) and Zuccarello et al. (2013), based on “randomised correlations”. In particular, this involved considering both a zero time difference between the seismic and emission rate time series, and testing different possible time lags (ranging from  $-10$  to  $10$  min). Infrasonic signals, recorded by the permanent infrasonic network, run by INGV, Osservatorio Etneo, were also analysed. However, wind noise at the sensors, obscured the volcano-acoustic signals to such an extent that no meaningful use of these data could be made.

## 4. Results

We measured 195 events over the acquisition period, which ranged  $\approx 0.1\text{--}14$  kg in  $\text{SO}_2$  mass corresponding to  $\approx 0.1\text{--}74$  kg in total gas mass per event, such that we estimate that  $\approx 183$  kg of  $\text{SO}_2$  and  $\approx 9.7 \times 10^2$  kg in gas overall were released explosively in this time window. In contrast, the total passive  $\text{SO}_2$  release was  $\approx 360$  kg in this interval, calculated by integrating the gas flux record over the time period, then subtracting the total explosive  $\text{SO}_2$  release. The ratio of passive to active degassing was therefore  $\approx 67\%$  passive:33% active.

A histogram of total gas masses for the explosions is shown in Fig. 4a, revealing a strong bias towards smaller masses, with a population of  $>150$  in the  $\approx 0.2\text{--}20$  kg range. The interval between event onsets ranged  $\approx 1\text{--}46$  s, with a modal value of  $\approx 4$  s and median of  $\approx 5$  s (Fig. 4b) and the duration of each event was  $<4$  s, Fig. 4c shows a plot of time from burst onset to that of the following slug, vs. total gas mass for each of the explosive events, revealing that for a given gas mass, there is a fixed time below which no subsequent gas burst was observed to occur (e.g., the shaded area in Fig. 4c). In contrast, Fig. 4d, a plot of time between burst onset and that of the preceding slug vs. total slug mass, reveals no such feature (Fig. 4d).

Furthermore, no significant link was found between the seismicity and gas flux time series data, suggesting that pressure and force change of the magma/gas mixture, within the conduit, were not strongly coupled to the edifice.

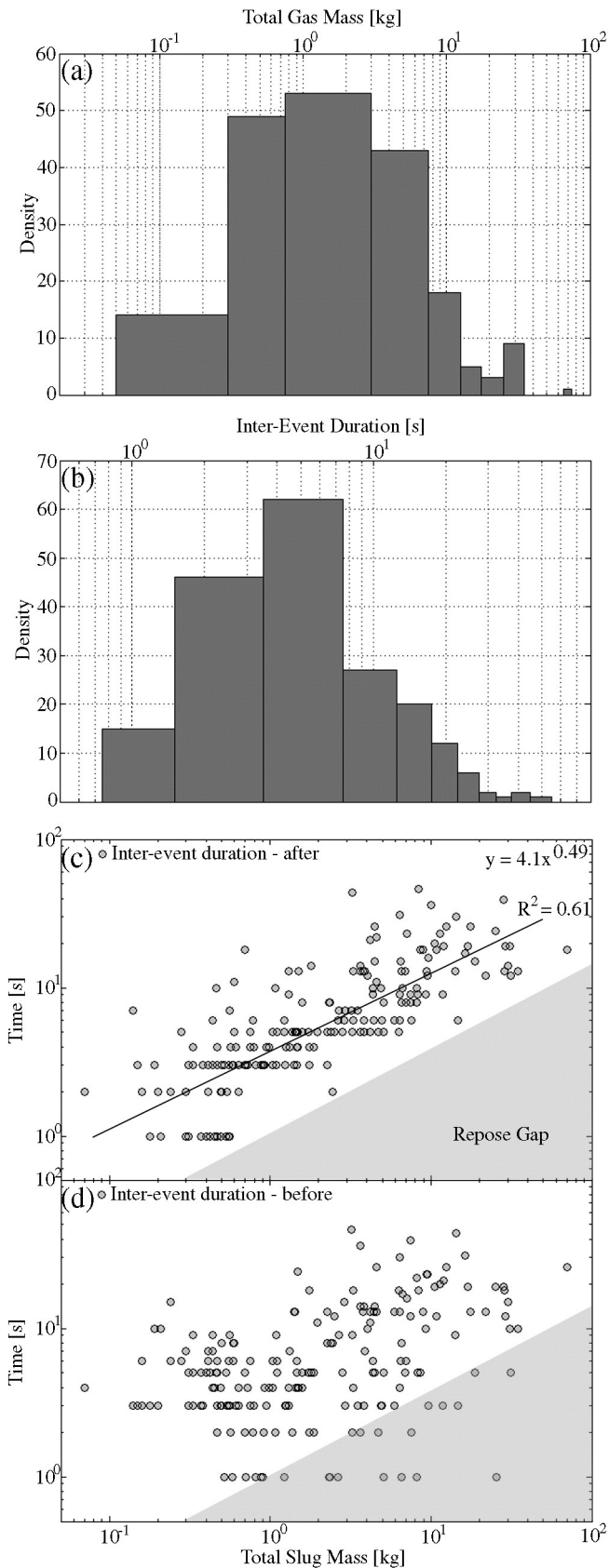


**Fig. 4.** Histograms showing a) the mass distribution of the erupted slugs; b) the inter-slug duration timing distribution (modal value of  $\approx 4$  s); log-log plots showing c) the inter-slug duration after each burst vs. that burst's gas mass, with a blank area indicated, termed the repose gap (discussed more fully in the text), and d) the inter-slug duration before each burst vs. that burst's gas mass.

## 5. Modelling

The first step in exploring the sub-surface processes driving the observed surficial activity is to consider which conduit flow regime might be operating in this case. By combining our estimated total gas masses with the ideal gas law ( $PV = nRT$ , where  $P$  is the gas pressure,  $V$  is the volume,  $n$  is the number of moles,  $R$  is the universal gas constant [ $\approx 8.314 \text{ J K}^{-1} \text{ mol}^{-1}$ ] and  $T$  is the temperature, respectively) at an atmospheric pressure of  $\approx 69 \text{ kPa}$  and temperature of  $1273.15 \text{ K}$  (e.g., an appropriate value for just above the magma surface), bubble volumes ranging  $\approx 0.4\text{--}411 \text{ m}^3$  are derived. Assuming a conduit radius of  $\approx 1 \text{ m}$ , that the bubbles are approximately as wide as the conduit, and that burst overpressure is of order one atmosphere, bubble lengths of  $\approx 0.1\text{--}53 \text{ m}$  are generated. Given that a bubble becomes a gas slug when bubble lengths exceed the conduit diameter (Davies and Taylor, 1950; Wallis, 1969), and a maximum film thickness is reached (e.g. Lewellin et al., 2012), criteria which the observed activity meet, we can potentially model the observed activity as being driven by bursting gas slugs.

Slugs consist of a quasi-hemispherical nose and a base of morphology (e.g. Fig. 5) dependent on the fluid dynamical regime (e.g., Davies

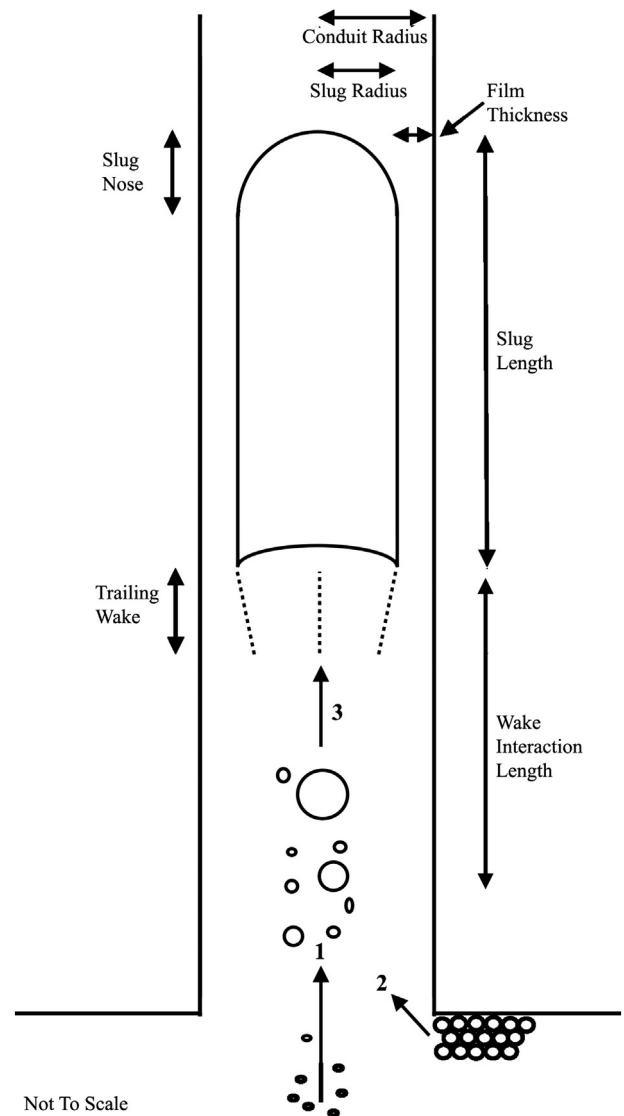


**Fig. 5.** Morphology of a gas slug, including the most important features. In addition, two possible slug formation theories are illustrated: 1) via coalescence of bubbles and 2) via the collapsing foam model.

and Taylor, 1950; Bendiksen, 1985; Campos and Guedes de Carvalho, 1988; Nogueira et al., 2006; Araújo et al., 2012). During the ascent process, the slug base has a relatively constant velocity, in contrast to the nose, which accelerates due to depressurisation induced volumetric expansion (James et al., 2006, 2008, 2009). An annular film of falling fluid surrounds the slug body, and is important in forming the trailing wake behind the slug, a feature that influences the coalescence of neighbouring slugs (Pinto and Campos, 1996) and contributes to the generation of turbulence (Krishna et al., 1999). Slug characteristics are controlled by conduit and magmatic parameters, which also determine the likelihood of bubble stability. The dimensionless inverse viscosity,  $N_f$ , can be used to investigate the properties of slugs as follows:

$$N_f = \frac{\rho_m}{\mu} \sqrt{g} (2r_c)^3 \quad (1)$$

where  $\rho_m$  is the magma density,  $\mu$  the magma dynamic viscosity,  $g$  the acceleration due to gravity and  $r_c$  the conduit radius. We assign a magmatic density of  $2600 \text{ kg m}^{-3}$  in line with the literature estimate of James et al. (2008) as being broadly representative of the bulk magma column (without slugs). Whilst we measured the vesicularity of a single ejectile clast (34%; collected during similar activity from the same vent on the 25th of July) we abstained from using this single datum to modify the above density estimate, given that this provided no constraint on vesicularity at depth. Furthermore, we found that our model runs were rather insensitive to uncertainty in density. For the remaining parameters we apply  $\mu = 100\text{--}1000 \text{ Pa s}$ ,  $g = 9.81 \text{ m s}^{-2}$  and  $r_c = 0.5\text{--}1.5 \text{ m}$ , in keeping with existing literature estimates for similar activity (e.g. Seyfried and Freundt, 2000), resulting in an  $N_f$  range of 8–423. According to Campos and Guedes de Carvalho (1988), for  $N_f$  values < 500 wakes will be closed and axi-symmetric such that turbulence is limited.

Another aspect to consider is the net magma motion and hence the validity of assuming a stagnant magma column as has been the case in previous volcanic slug flow models (e.g. James et al., 2008, 2009; Del Bello et al., 2012, in both cases concerning Stromboli). Based on visible observations of the activity (see visible imagery in the Supplementary material), the magmatic flux from the vent was negligible, hence, in common with the prior models, we also assume that there was no net vertical magmatic flux in this case.

In the absence of a previously developed model to characterise near-surface multi-slug flow, we resort to the single slug model of James et al. (2008), to probe first order estimates of the slug parameters. Following James et al. (2008) the position and length of an ascending slug as a function of time can be derived by numerically solving:

$$\frac{1}{2} \rho_m (1 + A') \ddot{L} = P_0 L_0^\gamma L^{-\gamma} h^{-1} - \rho g - P h^{-1} - 8\mu \dot{L} r_c^{-2} \quad (2)$$

where  $h$  is the height of magma overlying the slug nose,  $\gamma$  is the ratio of specific heats of the gas (here we use a value of 1.4) and  $L$  is the slug length, with zero subscripts indicating initial conditions and dots representing time derivatives. The initial gas pressure,  $P_0$ , is set to  $\rho_m g h_0 + P$  where  $h_0$  is the initial liquid height above the slug and  $P$  is the atmospheric pressure at the vent exit.  $A'$  is the squared ratio of the conduit and slug ( $r_{sl}$ ) radii:

$$A' = \left( \frac{r_{sl}}{r_c} \right)^2 \quad (3)$$

where  $r_{sl}$  is calculated by determining the thickness of the falling film  $\lambda'$  from Llewellyn et al. (2012) and subtracting this from  $r_c$ ;  $\lambda'$  is found from:

$$\lambda' = 0.204 + 0.123 \tanh(2.66 - 1.15 \log_{10} N_f) \quad (4)$$

$h$ , within Eq. (2), is a function of the constant rise velocity  $u_{sl}$  of the slug base:

$$u_{sl} = Fr \sqrt{2gr_c} \quad (5)$$

where the Froude number,  $Fr$ , appropriate for the given inertial-viscous regime is determined using the simplification of Llewellyn et al. (2012):

$$Fr = 0.34 \left[ 1 + \left( \frac{31.08}{N_f} \right)^{1.45} \right]^{-0.71} \quad (6)$$

The range of determined  $N_f$  values, 8–423, therefore gives estimates of film thickness of  $\approx 0.13$  to  $0.43 \text{ m}$ , and slug base velocities of  $\approx 0.24\text{--}1.82 \text{ m s}^{-1}$ .

We calculate the depth at which the ascending bubbles are sufficiently long to be considered as slugs by initialising the model at depths greater than this point (e.g., where bubble length is twice the conduit radius). Using mid-point values of  $1 \text{ m}$  for conduit radius and  $500 \text{ Pa s}^{-1}$  for viscosity (e.g.  $N_f = 46$ ,  $\lambda' = 0.28 \text{ m}$ , and  $u_{sl} = 1.1 \text{ m s}^{-1}$ ) this gives slug transition depths of  $\approx 170 \text{ m}$  for the largest slugs, and only  $\approx 5 \text{ m}$  for the vast majority of bursts within the median mass range (e.g. Fig. 5). Following this, we generate estimates of slug lengths at burst, using Eq. (2), of  $\approx 3\text{--}27 \text{ m}$ . By combining these constraints with estimates for slug rise speeds, we infer minimum rise times of  $\approx 93\text{--}708 \text{ s}$  from the slug transition depths to the surface for the largest slugs.

In a multi-slug regime, the dynamics will clearly be rather more complex than for single slugs (e.g. Pinto et al., 1998, 2001; Krishna et al., 1999). As such, there are a number of limits to using single slug models in our case, including the possibility that the rising slugs might not become conduit filling until closer to the surface than predicted by these models. Furthermore, slugs will be affected by pressure variations and magma motions induced by other slugs, and may coalesce with their neighbours. In a multi-slug system, slug base velocities can also exceed those predicted for single-slug systems (Krishna et al., 1999), with velocity fluctuations between individual slugs likely, which will further enhance slug interaction and the possibility of coalescence. Furthermore, whether the slug wakes are open or closed will play a significant role in determining whether turbulence occurs and whether rising slugs interact with their neighbours. Pinto and Campos (1996) provide the following relation (appropriate to the above  $N_f$  values) to characterise the distance beyond which no interaction occurs between rising slugs, termed the wake interaction length (e.g. see Fig. 5), and hence within which, inter-slug coalescence becomes likely:

$$l_{min} = 2r_c (1.46 + 4.75 \times 10^{-3} N_f) \quad (7)$$

This gives estimates of wake interaction lengths of  $\approx 1.5$  to  $10.4 \text{ m}$ , over the  $N_f$  range 8–423.

## 6. Discussion

### 6.1. Modelling and activity dynamics

The modelled slug wake interaction lengths ( $l_{min}$ ) of  $\approx 1.5$  to  $10.4 \text{ m}$  are suggestive that individual slugs could rise in the conduit separated by relatively little melt without interacting, so long as the slugs and their wakes retain stability. As a mass of gas rises through a conduit it will undergo decompressional expansion due to the reduction of overhead magma. When the gas mass transitions to become a slug, at a point when the slug length approaches the conduit diameter (Davies and Taylor, 1950; Wallis, 1969) and the maximum film thickness has been reached (e.g. Llewellyn et al., 2012), decompressional expansion of the slug length continues. The slug base rises at a constant velocity (Viana et al., 2003) whilst the nose accelerates towards the magma surface. Acceleration of the slug nose increases on approaching the

magma surface. This process therefore enhances the chance of coalescence between slugs, with slug interaction initiating around the interaction length, within which the whole of a trailing slug will accelerate into the base of a leading slug, whereby the slug base velocity, in tandem with the slug nose, will increase (e.g. Pinto and Campos, 1996) before complete capture at the point of coalescence. By combining our modelled slug interaction lengths of  $\approx 1.5$  to 10.4 m with estimates for slug base rise velocity of  $\approx 0.24$ – $1.82$  m s<sup>-1</sup>, and the mean delay between events of  $\approx 4$  s, we can estimate a separation distance between rising slugs of  $\approx 0.96$ – $2.2$  m, clearly within the modelled slug interaction lengths. It is therefore feasible that the observed rapid activity could occur with potential inter-slug interactions leading to slug coalescence events.

With a closed and axisymmetric wake, there will be little disruption of fluid following the passage of a rising slug. This could therefore allow the occurrence of the observed high frequency explosive activity via the bursting of individual gas slugs. However, it is possible that in a multi-slug environment, instability could still be generated by the extension of fluid disturbance beyond the estimated wake interaction length (e.g. Krishna et al., 1999). Given the inherently necessary estimates and assumptions for a number of parameters in our analysis, it is possible that the degree of turbulence has been under-represented, and that turbulent interaction of the magma–gas mixture with rising gas masses could lead to instability in rising masses causing homogeneous bubble morphology alterations. Despite this, the majority of bubbles, in the observed activity, are estimated to transition into slugs at relatively shallow depths in the conduit and  $N_f$  numbers of  $\approx 423$  suggest limited turbulence and hence relatively stable bubble morphology. Furthermore, our estimated final slug lengths of  $\approx 3$ – $27$  m for the majority of bursts are acquired through volumetric expansion, such that the largest masses, which have the greatest expansion, will be most prone to coalescence events.

In the Supplementary video data and Fig. 3 there is clear evidence of events occurring in very rapid succession, e.g., every few seconds around 09:55:33 GMT. In such cases, the gases from adjacent bubbles are propelled from the vent in markedly different directions. Whilst we cannot rule out the influence of factors such as vent geometry, atmospheric transport (e.g., eddy generation) and the magma surface itself (e.g., topographic alterations due to vent collapse or pyroclast deposit) in driving the explosive direction, we suggest that this observation could hypothetically be evidence of interaction of the trailing slug with the wake of the leading slug. This process can cause asymmetric deformation of the trailing slug's nose (e.g., Nogueira et al., 2006; Figueroa-Espinoza and Fabre, 2011), leading to a displacement in the explosive gas release vector.

Fig. 4c portrays a repose gap, such that the largest slugs are characterised by relatively long delays before the onset of the following event; no such feature is observed in terms of time before the bursts (Fig. 4d). We also suggest here that the most likely causative mechanism is slug coalescence, such that when a slug enters into the wake of the preceding Taylor bubble, it is accelerated towards the bubble base (Pinto et al., 1998, 2001). Therefore, during the high frequency strombolian activity reported on here, larger coalescence generated slugs could form from closely spaced rising Taylor bubbles. This would then leave a longer delay before the onset of the following event, e.g., explaining the repose gap. The absence of this feature prior to such bursts also supports this, in the sense that a slug has no influence on those preceding it.

We also considered whether other processes associated with strombolian volcanic dynamics might provide alternate explanations for this repose gap. In particular, the rise velocities of the base of slugs in a stagnant fluid are independent of mass (Viana et al., 2003), and are rather defined by conduit width (notwithstanding the effects of complex geometries and rheology). It is therefore unlikely that the rise speed-dependent model (Wilson, 1980; Parfitt and Wilson, 1995) could account for this phenomenon. This is of course unless the slug

arrival times could be effectively pre-determined by the volume-related behaviour of bubbles in the melt before the transition to slugs, given the estimated shallow transition depths.

The collapsing foam model (Jaupart and Vergnolle, 1988; Vergnolle and Brandeis, 1994), where bubbles in traps, or accumulated as a foam, collapse to generate slugs at variable temporal intervals was also considered, e.g., release of a large slug from a foam could lead to a longer period of stability before the next foam collapse event. However, as the foam collapse model is strongly related to storage, it could be more logical to expect this to cause longer inter-event durations before the largest eruptions, to allow sufficient gas accumulation in the foam/trap to take place, and as shown in Fig. 4d no such behaviour is evident. In view of all of the above we cautiously suggest that the repose gap is related to the coalescence of gas slugs, although, regardless of the precise driving mechanism, this observation does stand as both novel and intriguing.

## 6.2. Mass considerations and comparisons

Whilst 195 events were measured, we can of course only discuss the implications of our work with respect to the observation period, given the relatively limited acquisition duration. During the measurements, the captured SO<sub>2</sub> masses for individual bursts ranged  $\approx 0.1$ – $14$  kg, somewhat lower than those reported for strombolian explosions at other targets e.g., Stromboli  $\approx 15$ – $40$  kg (Mori and Burton, 2009) and  $\approx 2$ – $55$  kg (Tamburello et al., 2012); and Pacaya (3–29 kg) (Dalton et al., 2010). Our Etnean measurements demonstrate ratios of passive to active degassing of 67%:33% rather lower than those reported for Stromboli (77%: 23%; by Tamburello et al., 2012; 97–92%:3–8% by Mori and Burton, 2009), in line with the rather higher strombolian eruptive frequency in the former case e.g., on timescales of seconds vs. minutes. Indeed, strombolian activity on Mt. Etna, whilst relatively rare in comparison to the quasi-constant activity on Stromboli, does often manifest these rather shorter inter-eruptive periods (GVP, 2013), perhaps hinting at distinct mechanisms driving the eruptions in the two cases.

The relatively low gas masses released per event are also likely related to the weak seismic strength manifested at the time of observations (Fig. 2d), consistent with a mild form of strombolian activity and reduced gas supply from depth, in contrast to the stronger seismic events registered in the preceding hours (see Fig. 2d). Moreover, at the time of measurement the volcanic tremor source centroid was roughly located beneath Etna's North East crater at  $\approx 2$  km a.s.l. which likely masked any signal from the waning BN activity. Hence, whilst clear relationships between explosive gas masses and seismic signals have been reported previously at Mt. Etna (e.g. Zuccarello et al., 2013) and elsewhere e.g., on Stromboli and Asama volcanoes (McGonigle et al., 2009; Kazahaya et al., 2011) no correlation is evident here where the gas slugs are smaller. This is of course consistent with the model that seismo-volcanic signals (such as volcanic tremor, LP and VLP events) are generated by the slug and/or displaced magma moving within the conduit to generate a gas volume related seismic signal, possibly in a resonant manner (O'Brien and Bean, 2008), and adds credence to the near surface development of the observed activity.

## 7. Summary and conclusions

Here we report the use of UV cameras to constrain erupted gas masses during strombolian activity on Mt. Etna for the first time. Total gas masses per event of  $\approx 0.2$ – $74$  kg were captured, rather less than those found for this explosive style on other volcanoes, due to the mild, yet very frequent (i.e. every  $\approx 4$  s), form of activity. This is corroborated by the generally poor correlation with seismic signals, in contrast to the robust connections, evident elsewhere, for instance at Stromboli (Ripepe et al., 2005; McGonigle et al., 2009).

A broad consideration into the fluid dynamical regime intimates the potential for wake interaction between adjacent rising slugs, given their relatively modest separation in the conduit. We also report on an observed repose gap, in which the larger slugs have longer repose intervals than the smaller ones, before the following explosion. This could be indicative of slug coalescence, with the larger slugs being formed by the interaction between two or more slugs, leaving a relatively long delay before the arrival at the surface of the next distinct slug. We estimate that these bubbles transition to full slug flow at shallow depths of <170 m and that wake interaction becomes important in the upper portion of the conduit in the region of greatest vertical slug expansion, hence promoting coalescence.

## Acknowledgements

T.D. Pering and A.J.S. McGonigle acknowledge the support of a NERC studentship (x/007002-14), the University of Sheffield and a Google Faculty Research award (r/136958-11-1). A. Aiuppa acknowledges support from the European Research Council starting independent research grant (agreement number 1305377). We are finally grateful to the editor, Ed Llewellyn and two anonymous reviewers for their reviews which have greatly improved the quality of this paper.

## Appendix A. Supplementary data

Supplementary data associated with this article can be found in the online version, at <http://dx.doi.org/10.1016/j.jvolgeores.2014.12.013>. These data include Google map of the most important areas described in this article.

## References

- Aiuppa, A., Moretti, R., Federico, C., Giudice, G., Gurrieri, S., Luzzo, M., Papale, P., Shinohara, H., Valenza, M., 2007. Forecasting Etna eruptions by real-time observation of volcanic gas composition. *Geology* 35 (12), 1115–1118. <http://dx.doi.org/10.1130/G24149>.
- Araújo, J.D.P., Miranda, J.M., Pinto, A.M.F.R., Campos, J.B.L.M., 2012. Wide-ranging survey on the laminar flow of individual Taylor bubbles rising through stagnant Newtonian liquids. *Int. J. Multiphase Flow* 43, 131–148.
- Bendiksen, K.H., 1985. On the motion of long bubbles in vertical tubes. *Int. J. Multiphase Flow* 11 (6), 797–812.
- Blackburn, E.A., Wilson, L., Sparks, R.S.J., 1976. Mechanisms and dynamics of strombolian activity. *J. Geol. Soc. Lond.* 132, 429–440.
- Bluth, G.J.S., Shannon, J.M., Watson, I.M., Prata, A.J., Realmuto, V.J., 2007. Development of an ultra-violet digital camera for volcanic SO<sub>2</sub> imaging. *J. Volcanol. Geotherm. Res.* 161, 47–56.
- Boichu, M., Oppenheimer, C., Tsanev, V., Kyle, P.R., 2010. High temporal resolution SO<sub>2</sub> flux measurements at Erebus volcano, Antarctica. *J. Volcanol. Geotherm. Res.* 190, 325–336. <http://dx.doi.org/10.1016/j.jvolgeores.2009.11.020>.
- Burton, M., Allard, P., Muré, F., La Spina, A., 2007. Magmatic gas composition reveals the source depth of slug-driven strombolian explosive activity. *Science* 317, 227–230.
- Burton, M.R., Caltabiano, T., Mure, F., Salerno, G., Randazzo, D., 2009. SO<sub>2</sub> flux from Stromboli during the 2007 eruptions: results from the FLAME network and traverse measurements. *J. Volcanol. Geotherm. Res.* 183 (3–4), 214–220. <http://dx.doi.org/10.1016/j.jvolgeores.2008.11.025>.
- Campos, J.B.L.M., Guedes de Carvalho, J.R.F., 1988. An experimental study of the wake of gas slugs rising in liquids. *J. Fluid Mech.* 196, 27–37.
- Cannata, A., Di Grazia, G., Aliotta, M., Cassisi, C., Montalto, P., Patanè, D., 2013. Monitoring seismo-volcanic and infrasonic signals at volcanoes: Mt. Etna case study. *Pure Appl. Geophys.* <http://dx.doi.org/10.1007/s00024-012-0634-x>.
- Chouet, B., Hamisevi, N., McGetchi, T.R., 1974. Photoballistics of volcanic jet activity at Stromboli, Italy. *J. Geophys. Res.* 79 (32), 4961–4976.
- Dalton, M.P., Waite, G.P., Watson, I.M., Nadeau, P.A., 2010. Multiparameter quantification of gas release during weak strombolian eruptions at Pacaya volcano, Guatemala. *Geophys. Res. Lett.* 37 (L09303). <http://dx.doi.org/10.1029/2010GL042617>.
- Davies, R.M., Taylor, G.I., 1950. The mechanics of large bubbles rising through extended liquids and through liquids in tubes. *Proc. R. Soc. Lond. A200*, 375–390.
- Del Bello, E., Llewellyn, E.W., Taddeucci, J., Scarlato, P., Lane, S.J., 2012. An analytical model for gas overpressure in slug-drive explosions: insights into strombolian volcanic eruptions. *J. Geophys. Res. Solid Earth* 117 (B2). <http://dx.doi.org/10.1029/2011JB008747>.
- Edmonds, M., Herd, R.A., Galle, B., Oppenheimer, C.M., 2003. Automated, high time-resolution measurements of SO<sub>2</sub> flux at Soufrière Hills Volcano, Montserrat. *Bull. Volcanol.* 65 (8), 578–586.
- Figuerao-Espinoza, B., Fabre, J., 2011. Taylor bubble moving in a flowing liquid in vertical channel: transition from symmetric to asymmetric shape. *J. Fluid Mech.* 679, 432–454.
- Galle, B., Oppenheimer, C., Geyer, A., McGonigle, A.J.S., Edmonds, M., Horrocks, L., 2003. A miniaturised ultraviolet spectrometer for remote sensing of SO<sub>2</sub> fluxes: a new tool for volcano surveillance. *J. Volcanol. Geotherm. Res.* 119 (1–4), 241–254. [http://dx.doi.org/10.1016/S0377-0273\(02\)00356-6](http://dx.doi.org/10.1016/S0377-0273(02)00356-6).
- GVP, 2013. Etna. (Online) Available at: <http://www.volcano.si.edu/volcano.cfm?vn=211060>.
- Hendrix, A.R., Vilas, F., Festou, M.C., 2003. Vesta's UV lightcurve: hemispheric variation in brightness and spectral reversal. *Icarus* 162 (1), 1–9.
- Holland, A.S.P., Watson, M.I., Phillips, J.C., Caricchi, L., Dalton, M.P., 2011. Degassing processes during lava dome growth: insights from Santiaguito lava dome, Guatemala. *J. Volcanol. Geotherm. Res.* 202 (1–2), 153–166. <http://dx.doi.org/10.1016/j.jvolgeores.2011.02.004>.
- James, M.R., Lane, S.J., Chouet, B., Gilbert, J.S., 2004. Pressure changes associated with the ascent and bursting of gas slugs in liquid-filled vertical and inclined conduits. *J. Volcanol. Geotherm. Res.* 129, 61–82. [http://dx.doi.org/10.1016/S0377-0273\(03\)00232-4](http://dx.doi.org/10.1016/S0377-0273(03)00232-4).
- James, M.R., Lane, S.J., Chouet, B.A., 2006. Gas slug ascent through changes in conduit diameter: laboratory insights into a volcano-seismic source process in low-viscosity magmas. *J. Geophys. Res.* 111 (B05201). <http://dx.doi.org/10.1029/2005JB003718>.
- James, M.R., Lane, S.J., Corder, S.B., 2008. Modelling the rapid near-surface expansion of gas slugs in low-viscosity magmas. *Geol. Soc. Lond., Spec. Publ.* 307, 147–167.
- James, M.R., Lane, S.J., Wilson, L., Corder, S.B., 2009. Degassing at low magma-viscosity volcanoes: quantifying the transition between passive bubble-burst and strombolian eruption. *J. Volcanol. Geotherm. Res.* 180, 81–88.
- Jaupart, C., Vergnolle, S., 1988. Laboratory models of Hawaiian and strombolian eruptions. *Nature* 331, 58–60.
- Kantzas, E.P., McGonigle, A.J.S., Tamburello, G., Aiuppa, A., Bryant, G., 2010. Protocols for UV camera volcanic SO<sub>2</sub> measurements. *J. Volcanol. Geotherm. Res.* 194, 55–60.
- Kazahaya, R., Mori, T., Takeo, M., Ohminato, T., Urabe, T., Maeda, Y., 2011. Relation between single very-long-period pulses and volcanic gas emissions at Mt. Asama, Japan. *Geophys. Res. Lett.* 38 (L11307). <http://dx.doi.org/10.1029/2011GL047555>.
- Kern, C., Deutschmann, T., Vogel, L., Wöhrbach, M., Wagner, T., Platt, U., 2009. Radiative transfer corrections for accurate spectroscopic measurements of volcanic gas emissions. *Bull. Volcanol.* 72, 233–247. <http://dx.doi.org/10.1007/s00445-009-0313-7>.
- Kern, C., Kick, F., Lübcke, P., Vogel, L., Wöhrbach, M., Platt, U., 2010. Theoretical description of functionality, applications, and limitations of SO<sub>2</sub> cameras for the remote sensing of volcanic plumes. *Atmos. Meas. Tech.* 3, 733–749. <http://dx.doi.org/10.5194/amt-3-733-2010>.
- Krishna, R., Urseanu, M.I., van Baten, J.M., Ellenberger, J., 1999. Rise velocity of a swarm of large gas bubbles in liquids. *Chem. Eng. Sci.* 54, 171–183.
- La Spina, A., Burton, M.R., Harig, R., Mure, F., Rusch, P., Jordan, M., Caltabiano, T., 2013. New insights into volcanic processes at Stromboli from Cerberus, a remote-controlled open-path FTIR scanner system. *J. Volcanol. Geotherm. Res.* 249, 66–76.
- Lane, S.J., James, M.R., Corder, S.B., 2013. Volcanic infrasonic signals and magma degassing: first-order experimental insights and application to Stromboli. *Earth Planet. Sci. Lett.* 377–378, 169–179. <http://dx.doi.org/10.1016/j.epsl.2013.06.048>.
- Llewellyn, E.W., Del Bello, E., Taddeucci, J., Scarlato, P., Lane, S.J., 2012. The thickness of the falling film of liquid around a Taylor bubble. *Proc. R. Soc. B* 468. <http://dx.doi.org/10.1098/rspa.2011.0476>.
- Martini, F., Bean, C.J., Saccorotti, G., Viveiros, F., Wallenstein, N., 2009. Seasonal cycles of seismic velocity variations detected using coda wave interferometry at Fogo volcano, São Miguel, Azores, during 2003–2004. *J. Volcanol. Geotherm. Res.* 181, 231–246.
- McGonigle, A.J.S., Hilton, D.R., Fischer, T.P., Oppenheimer, C., 2005. Plume velocity determination for volcanic SO<sub>2</sub> flux measurements. *Geophys. Res. Lett.* 32 (L11302). <http://dx.doi.org/10.1029/2005GL022470>.
- McGonigle, A.J.S., Aiuppa, A., Ripepe, M., Kantzas, E.P., Tamburello, G., 2009. Spectroscopic capture of 1 Hz volcanic SO<sub>2</sub> fluxes and integration with volcano geophysical data. *Geophys. Res. Lett.* 36 (L21309). <http://dx.doi.org/10.1029/2009GL040494>.
- Mori, T., Burton, M., 2006. The SO<sub>2</sub> camera: a simple, fast and cheap method for ground-based imaging of SO<sub>2</sub> in volcanic plumes. *Geophys. Res. Lett.* 33 (L24804). <http://dx.doi.org/10.1029/2006GL027916>.
- Mori, T., Burton, M., 2009. Quantification of the gas mass emitted during single explosions on Stromboli with the SO<sub>2</sub> imaging camera. *J. Volcanol. Geotherm. Res.* 188, 395–400.
- Nogueira, S., Riethmuller, M.L., Campos, J.B.L.M., Pinto, A.M.F.R., 2006. Flow patterns in the wake of a Taylor bubble rising through vertical columns of stagnant and flowing Newtonian liquids: an experimental study. *Chem. Eng. Sci.* 61, 7199–7212.
- O'Brien, G.S., Bean, C.J., 2008. Seismicity on volcanoes generated by gas slug ascent. *Geophys. Res. Lett.* 25 (L16308). <http://dx.doi.org/10.1029/2008GL035001>.
- Parfitt, E.A., Wilson, L., 1995. Explosive volcanic eruptions – IX. The transition between Hawaiian-style lava fountaining and strombolian explosive activity. *Geophys. J. Int.* 121 (1), 226–232.
- Pering, T.D., Tamburello, G., McGonigle, A.J.S., Aiuppa, A., Cannata, A., Giudice, G., Patanè, D., 2014. High time resolution fluctuations in volcanic carbon dioxide degassing from Mount Etna. *J. Volcanol. Geotherm. Res.* 270, 115–121. <http://dx.doi.org/10.1016/j.jvolgeores.2013.11.014>.
- Pinto, A.M.F.R., Campos, J.B.L.M., 1996. Coalescence of two gas slugs rising in a vertical column of liquid. *Chem. Eng. Sci.* 51 (1), 45–54.
- Pinto, A.M.F.R., Coelho Pinheiro, M.N., Campos, J.B.L.M., 1998. Coalescence of two gas slugs rising in a co-current flowing liquid in vertical tubes. *Chem. Eng. Sci.* 53 (16), 2973–2983.
- Pinto, A.M.F.R., Coelho Pinheiro, M.N., Campos, J.B.L.M., 2001. On the interaction of Taylor bubbles rise in two-phase co-current slug flow in vertical columns: turbulent wakes. *Exp. Fluids* 31, 643–652.



- Pioli, L., Bonadonna, C., Azzopardi, B.J., Phillips, J.C., Ripepe, M., 2012. Experimental constraints on the outgassing dynamics of basaltic magmas. *J. Geophys. Res.* 117 (B03204). <http://dx.doi.org/10.1029/2011JB008392>.
- Ripepe, M., Marchetti, E., Ulvieri, G., Harris, A., Dehn, J., Burton, M., Caltabiano, T., Salerno, G., 2005. Effusive to explosive transition during the 2003 eruption of Stromboli volcano. *Geology* 33 (5), 341–344.
- Ripepe, M., Delle Donne, D., Harris, A., Marchetti, E., Olivieri, G., 2008. Stromboli volcano: an integrated study of the 2002–2003 eruption. In: Calvari, S., Inguaggiato, S., Puglisi, G., Ripepe, M., Rosi, M. (Eds.), *Dynamics of Strombolian Activity*. Geophysical Monograph Series 182, pp. 39–48. <http://dx.doi.org/10.1029/182GM05>.
- Seyfried, R., Freundt, A., 2000. Experiments on conduit flow and eruption behaviour of basaltic volcanic eruptions. *J. Geophys. Res.* 105 (B10), 23,727–23,740.
- Tamburello, G., Kantzas, E.P., McGonigle, A.J.S., Aiuppa, A., 2011a. Recent advances in ground-based ultraviolet remote sensing of volcanic SO<sub>2</sub> fluxes. *Ann. Geophys.* 54 (2), 199–208.
- Tamburello, G., Kantzas, E.P., McGonigle, A.J.S., Aiuppa, A., 2011b. Vulcamera: a program for measuring volcanic SO<sub>2</sub> using UV cameras. *Ann. Geophys.* 54 (2), 219–221.
- Tamburello, G., Aiuppa, A., Kantzas, E.P., McGonigle, A.J.S., Ripepe, M., 2012. Passive vs. active degassing modes at an open-vent volcano (Stromboli, Italy). *Earth Planet. Sci. Lett.* 359–360, 106–116.
- Tamburello, G., Aiuppa, A., McGonigle, A.J.S., Allard, P., Cannata, A., Giudice, G., Kantzas, E.P., Pering, T.D., 2013. Periodic volcanic degassing behaviour: the Mount Etna example. *Geophys. Res. Lett.* 40 (18), 4818–4822. <http://dx.doi.org/10.1002/grl.50924>.
- Vergnolle, S., Brandeis, G., 1994. Origin of the sound generated by strombolian explosions. *Geophys. Res. Lett.* 21 (18), 1959–1962.
- Vergnolle, S., Brandeis, G., 1996. Strombolian explosions: a large bubble breaking at the surface of a lava column as a source of sound. *J. Geophys. Res.* 101, 20,433–20,448.
- Viana, F., Pardo, R., Yáñez, R., Trallero, J.L., Joseph, D.D., 2003. Universal correlation for the rise velocity of long gas bubbles in round pipes. *J. Fluid Mech.* 494, 379–398.
- Wallis, G.B., 1969. *One-dimensional Two-phase Flow*. McGraw-Hill, New York, NY.
- Williams-Jones, G., Horton, K.A., Elias, T., Garbeil, H., Mouginiis-Mark, P.J., Sutton, A.J., Harris, A.J.L., 2006. Accurately measuring volcanic plume velocity with multiple UV spectrometers. *Bull. Volcanol.* 68, 328–332.
- Wilson, L., 1980. Relationships between pressure, volatile content, and ejecta velocity in three types of volcanic explosions. *J. Volcanol. Geotherm. Res.* 8, 297–313.
- Zuccarello, L., Burton, M.R., Saccorotti, G., Bean, C.J., Patanè, D., 2013. The coupling between very long period seismic events, volcanic tremor, and degassing rates at Mount Etna volcano. *J. Geophys. Res. Solid Earth* 118, 4910–4921. <http://dx.doi.org/10.1002/jgrb.50363>.